Inorganic Chemistry
Article

Inorg. Chem. **2009**, *48*, 10913–10925 **10913**
DOI: 10.1021/ic9008976

Square Planar Bis{3,6-bis(trimethylsilyl)benzene-1,2-dithiolato}metal Complexes of Cr^{II}, Co^{III}, and Rh^{II}: An Experimental and Density Functional Theoretical Study

Flávio Luiz Benedito, Taras Petrenko, Eckhard Bill, Thomas Weyhermüller, and Karl Wieghardt*

Max-Planck-Institut für Bioanorganische Chemie, Stiftstrasse 34-36, D-45470 Mülheim an der Ruhr, Germany

Received May 8, 2009

The three square planar complexes $[N(n\text{-}Bu)_4]_2[Cr^{II}L_2]\cdot 4CH_3CN$ (S=2; **1**), $[N(n\text{-}Bu)_4][Co^{III}L_2]$ (S=1; **3**), and $[N(n\text{-}Bu)_4]_2[Rh^{II}L_2]\cdot 4CH_3CN$ ($S = {}^1/_2$; **4**) have been prepared and structurally characterized by X-ray crystallography (L^{2-} represents the 3,6-bis(trimethylsilyl)benzene-1,2-dithiolate(2−)). Aerial oxidation of CH_2Cl_2 solutions of **1** produced purple crystals of $[N(n\text{-}Bu)_4][Cr^{V}OL_2]\cdot 2CH_2Cl_2$ ($S={}^1/_2$; **2**), the structure of which has also been determined by X-ray crystallography. The electro- and magnetochemistry of all species has been studied. Their electronic structures have been experimentally investigated by recording their electronic and EPR spectra; solid-state temperature-dependent magnetic susceptibility measurements have been performed. Density functional theoretical calculations at the ZORA-B3LYP level have been carried out for all four species in order to obtain a better understanding of the electronic structure of the square planar complexes and the one-electron reduced $[Rh^{I}L_2]^{3-}$ species. The reactivity of the latter with CH_3I has been studied, and two products have been identified: *cis*-$[Rh^{III}I_2(L'')(L')]$ and *cis*-$[Rh^{III}(CH_3)(I)(L'')(L')]$ where $(L')^-$ represents the S-methylated monoanion of L^{2-} and $(L'')^0$ is the neutral, twice-S-methylated form of $(L)^{2-}$.

Introduction

Relatively few bis(dithiolene)metal complexes containing early or middle transition metal ions have been characterized in the past.[1] This is in stark contrast to the now well-developed chemistry of such compounds with the late transition metal ions (Ni, Pd, Pt, Cu, Au, and Zn).[1]

The only structurally characterized species containing chromium(II) ions are $[NEt_4]_2[Cr^{II}(S_2C_2H_4)_2]$,[2] containing two saturated ethane-1,2-dithiolate(2−) ligands, and $[NEt_4]_2[Cr^{II}(S_2C_6H_4)_2]$, in which two benzene-1,2-dithiolate-(2−) ligands are S,S'-coordinated.[3] The geometry of the CrS_4 core in both compounds is square planar. The electronic structure of the former has been shown to encompass a high-spin Cr^{II} (d^4; S=2) ion. No magnetic or spectroscopic data for the second species have been reported to date.

$[N(n\text{-}Bu)_4]_2[Rh(mnt)_2]$[4,5] represents the only well-characterized monomeric, square planar bis(dithiolene)metal species of rhodium(II) where $(mnt)^{2-}$ is 1,2-maleonitrile-1,2-dithiolate(2−). It possesses an $S={}^1/_2$ ground state. Although the crystal structure has not been reported, the presence of its square planar, monomeric dianion $[Rh(mnt)_2]^{2-}$ has been deduced from its electron paramagnetic resonance (EPR) spectrum, magnetic moment (μ_{eff} = 1.9 μ_B), and X-ray powder diffraction pattern, which is isomorphous with that of structurally characterized $[N(n\text{-}Bu)_4]_2[Ni(mnt)_2]$.[4] Recently, we have reported[6] the synthesis of a new sterically demanding benzene-1,2-dithiolate(2−) ligand, namely, the disodium salt of 3,6-bis(trimethylsilyl)benzene-1,2-dithiolate(2−), Na_2L (Scheme 1). In coordination compounds, the ligand is generally bidentate, S,S'-coordinated to the given metal ion. The two coordinated sulfur donor atoms are sterically well protected by the two trimethylsilyl groups in the *ortho* position, thereby preventing effectively dimerization reactions of square planar bis(dithiolato)metal entities.

Here, we report the synthesis and molecular structures of three new square planar complexes of Cr, Co, and Rh, shown in Scheme 1. We have studied their electrochemistry and electronic structures in detail through magnetic susceptibility measurements and recorded their X-band EPR and electronic spectra. In addition, we have performed density functional theoretical (DFT) calculations to validate our electronic structure proposals.

*To whom correspondence should be addressed. E-mail: wieghardt@mpi-muelheim.mpg.de.

(1) Stiefel, E. I. *Prog. Inorg. Chem.* **2004**, *52*, 60.
(2) (a) Rao, C. P.; Dorfman, J. R.; Holm, R. H. *Inorg. Chem.* **1985**, *24*, 453. (b) Rao, C. P.; Dorfman, J. R.; Holm, R. H. *Inorg. Chem.* **1986**, *25*, 428.
(3) Sellmann, D.; Wille, M.; Knoch, F. *Inorg. Chem.* **1993**, *32*, 2534.
(4) Billig, E.; Shupack, S. I.; Waters, J. H.; Williams, R.; Gray, H. B. *J. Am. Chem. Soc.* **1964**, *86*, 926.
(5) Maki, A. H.; Edelstein, N.; Davison, A.; Holm, R. H. *J. Am. Chem. Soc.* **1964**, *86*, 4580.
(6) Pap, J. S.; Benedito, F. L.; Bothe, E.; Bill, E.; DeBeer George, S.; Weyhermüller, T.; Wieghardt, K. *Inorg. Chem.* **2007**, *46*, 4187.

Published on Web 10/15/2009

Scheme 1. Ligand and Complexes of This Work

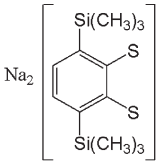

$Na_2(L)$

$[N(n\text{-}Bu)_4]_2[Cr^{II}L_2]\cdot 4CH_3CN$	S = 2	(**1**)
$[N(n\text{-}Bu)_4][Cr^{V}OL_2]\cdot 2CH_2Cl_2$	S = ½	(**2**)
$[N(n\text{-}Bu)_4][Co^{III}L_2]$	S = 1	(**3**)
$[N(n\text{-}Bu)_4]_2[Rh^{II}L_2]\cdot 4CH_3CN$	S = ½	(**4**)

Experimental Section

Preparations. The ligand disodium-3,6-bis(trimethylsilyl)-benzene-1,2-dithiolate, Na_2L, has been prepared as described in ref 6 and $[Rh_2(CH_3CN)_{10}](BF_4)_4$ as in ref 7.

$[N(n\text{-}Bu)_4]_2[Cr^{II}L_2]\cdot 4CH_3CN$ (1). To a solution of the ligand Na_2L (150 mg; 0.5 mmol) in degassed acetonitrile (10 mL) was added $[Cr^{II}(CH_3CN)_4](BF_4)_2$ (100 mg; 0.26 mmol), 1 mL (1 mmol) of lithiumtriethylborohydride (1 M solution in tetrahydrofurane), and $[N(n\text{-}Bu)_4]I$ (145 mg; 0.39 mmol). The mixture was stirred under an Ar blanketing atmosphere for 4 h at 20 °C, after which time a brownish-green solution was obtained, which was filtered. Orange crystals of $[N(n\text{-}Bu)_4]_2[Cr-L_2]\cdot 4CH_3CN$, suitable for X-ray analysis, grew from this solution at −30 °C. Yield: 256 mg (78%). Anal. Calcd for $C_{64}H_{124}N_6CrS_4Si_4$: C, 60.62; H, 9.72; N, 6.70; Cr, 4.12. Found: C, 60.58; H, 9.74; N, 6.68; Cr, 4.10.

$[N(n\text{-}Bu)_4][Cr^{V}OL_2]\cdot 2CH_2Cl_2$ (2). A solution of **1** (50 mg; 39 μmol) in CH_3CN (5 mL) was exposed to the air at 20 °C. The color of the solution changed immediately to purple. Removal of the solvent by evaporation in vacuo and redissolving in CH_2Cl_2 produced after 5 days at −20 °C purple crystals of **2**. Yield: 38 mg (93%). Anal. Calcd for $C_{42}H_{80}Cl_4CrNOS_4Si_4$ (dried sample): C, 48.02; H, 7.68; N, 1.33. Found: C, 48.10; H, 7.55; N, 1.21.

$[N(n\text{-}Bu)_4][Co^{III}L_2]$ (3). To a solution of the ligand Na_2L (150 mg; 0.5 mmol) in degassed dry methanol (25 mL) was added under anaerobic conditions, dropwise, a solution of $Co(CH_3CO_2)_2\cdot 4H_2O$ (65 mg; 0.26 mmol) and $[N(n\text{-}Bu)_4]I$ (145 mg; 0.39 mmol) in methanol (5 mL). The solution was stirred for 2 h at 20 °C, after which time it was exposed to the air. A color change from light green to deep blue was observed. The solvent was removed by evaporation in vacuo, and the blue residue was redissolved in acetonitrile. Dark blue crystals of **3** were obtained at −20 °C. Yield: 213 mg (94%). Anal. Calcd for $C_{40}H_{76}CoNS_4Si_4$: C, 58.20; H, 8.79; N, 1.61. Found: C, 58.32; H, 8.73; N, 1.65.

$[N(n\text{-}Bu)_4]_2[Rh^{II}L_2]\cdot 4CH_3CN$ (4). To a degassed acetonitrile solution (10 mL) of the ligand Na_2L (150 mg; 0.5 mmol) was added dropwise under anaerobic conditions (Ar) a degassed acetonitrile solution (5 mL) of $[Rh_2(CH_3CN)_{10}](BF_4)_4$ and $[N(n\text{-}Bu)_4]I$ (145 mg; 0.39 mmol) at 20 °C. After stirring for 4 h, a brownish-red solution was obtained, which was filtered through Celite and concentrated in vacuo to ~3 mL. Dark-red crystals of **4** were obtained at −30 °C. Yield: 170 mg (67%). Anal. Calcd for $C_{64}H_{124}N_6RhS_4Si_4$: C, 58.13; H, 9.45; N. 6.36. Found: C, 58.12; H, 9.45; N. 6.34.

Physical Measurements. Electronic absorption spectra of the complexes and spectra from the spectroelectrochemical measurements were recorded on an HP 8452A diode array spectrophotometer (range of 200−1100 nm). Cyclic voltammograms and coulometric electrochemical experiments were performed with an EG&G potentiostat/galvanostat. Temperature-dependent (2−298 K) magnetization data were recorded with a SQUID magnetometer (MPMS Quantum Design) in an external magnetic field of 1 T. The experimental magnetic susceptibility data were corrected for underlying diamagnetism using tabulated Pascal's constants. X-band EPR spectra were recorded with a Bruker ESP 300 spectrometer.

X-Ray Crystallographic Data Collection and Refinement of the Structures. An orange single crystal of $\mathbf{1}\cdot 4CH_3CN$, a red crystal of $\mathbf{2}\cdot 2CH_2Cl_2$, a blue specimen of **3**, and a dark red crystal of $\mathbf{4}\cdot 4CH_3CN$ were coated with perfluoropolyether, picked up with nylon loops, and were immediately mounted in the nitrogen cold stream of a Bruker-Nonius Kappa-CCD diffractometer equipped with a Mo-target rotating-anode X-ray source (Mo Kα radiation, $\lambda = 0.71073$ Å) and a graphite monochromator. Final cell constants were obtained from least-squares fits of all measured reflections. Intensity data were corrected for absorption using intensities of redundant reflections with the program SADABS.[8] The structures were readily solved by Patterson methods and subsequent difference Fourier techniques. The Siemens ShelXTL[9a] software package was used for solution and artwork of the structures; ShelXL97[9b] was used for the refinement. All non-hydrogen atoms were anisotropically refined, and hydrogen atoms were placed at calculated positions and refined as riding atoms with isotropic displacement parameters.

A CH_2Cl_2 solvent molecule in crystals of $\mathbf{2}\cdot 2CH_2Cl_2$ was found to be disordered. A split atom model with restrained anisotropic displacement parameters and bond distances using the EADP and SAME instructions of ShelXL97 was employed. The occupation ratio refined to about 0.72:0.28. Crystallographic data of the compounds are summarized in Table 1.

Calculations. All calculations in this work were performed with the electronic structure program package ORCA.[10] As will be further discussed in the text, the geometry optimizations were carried out at the B3LYP level[11,16] of DFT. The present calculations have been performed with inclusion of scalar relativistic effects at the second-order Douglas−Kroll−Hess level (DKH2).[12] In the geometry optimizations, the one-center approximation was used, which eliminates DKH2 contributions to the analytic gradients. In the context of ZORA,[13a] the one-center approximation has been shown to introduce only minor errors to the final geometries.[13b] Large uncontracted Gaussian basis sets, which were derived from the well-tempered basis sets of Huzinaga et al.,[14] were used at the metal center. For the remaining atoms, the all-electron polarized triple-ξ (TZVP)[15] Gaussian basis sets of Ahlrich's group were used; they were further uncontracted to allow for a distortion of the inner-shell orbitals in the presence of the relativistic potential.

The property calculations at the optimized geometries were done with the B3LYP functional.[16] In this case, the same basis

(7) Prater, M. E.; Pence, L. E.; Clérac, R.; Finniss, G. M.; Campana, C.; Auban-Senzier, P.; Jérome, D.; Canadell, E.; Dunbar, K. R. *J. Am. Chem. Soc.* **1999**, *121*, 8005.

(8) Sheldrick, G. M. *SADABS*, version 2006/1; Universität Göttingen: Göttingen, Germany, 2006.

(9) (a) *ShelXTL 6.14*; Bruker AXS Inc.: Madison, WI, 2003. (b) Sheldrick, G. M. *ShelXL97*; Universität Göttingen: Göttingen, Germany, 1997.

(10) Neese, F. *ORCA*, version 2.4, revision 16; Max-Planck-Institut für Bioanorganische Chemie: Mülheim, Germany, 2004.

(11) (a) Becke, A. D. *J. Chem. Phys.* **1988**, *84*, 4524. (b) Perdew, J. P. *Phys. Rev. B* **1986**, *33*, 8522.

(12) Hess, B. A.; Marian, C. M. In *Computational Molecular Spectroscopy*; Jensen, P., Bunker, P. R., Eds., John Wiley & Sons: New York, 2000; p 169.

(13) (a) van Lenthe, E.; Snijders, J. G.; Baerends, E. J. *J. Chem. Phys.* **1996**, *105*, 6505. (b) van Lenthe, J. H.; Faas, S.; Snijders, J. G. *Chem. Phys. Lett.* **2000**, *328*, 107.

(14) (a) Huzinaga, S.; Miguel, B. *Chem. Phys. Lett.* **1990**, *175*, 289. (b) Huzinaga, S.; Klobukowski, M. *Chem. Phys. Lett.* **1993**, *212*, 260.

(15) (a) Schäfer, A.; Horn, H.; Ahlrichs, R. *J. Chem. Phys.* **1992**, *97*, 2571. (b) Schäfer, A.; Huber, C.; Ahlrichs, R. *J. Chem. Phys.* **1994**, *100*, 5289.

(16) (a) Lee, C.; Yang, W.; Parr, R. G. *Phys. Rev. B* **1988**, *37*, 785. (b) Becke, A. D. *J. Chem. Phys.* **1993**, *98*, 5648.

Table 1. Crystallographic Data for **1**·4 CH_3CN, **2**·2 CH_2Cl_2, **3**, and **4**·4 CH_3CN

	1·4 CH_3CN	**2**·2 CH_2Cl_2	**3**	**4**·4 CH_3CN
chem. formula	$C_{64}H_{124}CrN_6S_4Si_4$	$C_{42}H_{80}Cl_4CrNS_4Si_4O$	$C_{40}H_{76}CoNS_4Si_4$	$C_{64}H_{124}N_6RhS_4Si_4$
fw	1270.29	1049.47	870.55	1321.20
space group	$P\bar{1}$, No. 2	$P2_1/c$, No. 14	$P\bar{1}$, No. 2	$P\bar{1}$, No. 2
a, Å	14.4962(6)	26.038(2)	11.8504(8)	12.6822(6)
b, Å	14.7533(6)	12.0821(6)	13.840(1)	13.0168(7)
c, Å	19.0960(8)	17.9404(8)	16.703(1)	13.3739(7)
α, deg	80.243(4)	90	112.590(3)	69.060(4)
β, deg	81.856(4)	98.691(4)	91.552(3)	67.672(4)
γ, deg	74.004(4)	90	98.818(3)	88.844(4)
V, Å	3849.6(3)	5579.1(6)	2488.3(3)	1890.2(2)
Z	2	4	2	1
T, K	100(2)	100(2)	100(2)	100(2)
ρ calcd, g cm^{-3}	1.069	1.249	1.162	1.161
refl. collected/$2\Theta_{max}$	67365/52.00	37991/55.00	43520/60.00	35348/65.00
unique reflns/$I > 2\sigma(I)$	15106/11336	12788/9287	14486/9820	13615/11315
no. of params/restr.	736/0	540/3	470/0	370/0
λ, Å/μ(Kα), cm^{-1}	0.71073/3.57	0.71073/6.63	0.71073/6.35	0.71073/4.39
R1[a]/goodness of fit[b]	0.0659/1.147	0.0440/1.037	0.0596/1.059	0.0450/1.063
wR2[c] ($I > 2\sigma(I)$)	0.1626	0.0779	0.0899	0.0920
residual density, e $Å^{-3}$	+1.19/−0.49	+0.47/−0.48	+0.47/−0.46	+0.73/−0.70

[a] Observation criterion: $I > 2\sigma(I)$. $R1 = \sum||F_o| - |F_c||/\sum|F_o|$. [b] $GoF = [\sum[w(F_o^2 - F_c^2)^2]/(n-p)]^{1/2}$. [c] $wR2 = [\sum[w(F_o^2 - F_c^2)^2]/\sum[w(F_o^2)^2]]^{1/2}$, where $w = 1/\sigma^2(F_o^2) + (aP)^2 + bP$, $P = (F_o^2 + 2F_c^2)/3$.

sets were used, but the quasi-relativistic ZORA method[13] was used because, in this formalism, the magnetic properties are more readily formulated.[17] For the calculation of the EPR parameters, the Fermi contact and the dipolar and metal spin−orbit contributions are included. TD-DFT calculations were carried out according to ref 18.

Results

1. Preparation of Complexes. The reaction of one-half of an equivalent of $[Cr^{II}(CH_3CN)_4](BF_4)_2$ and 1 equiv of the disodium salt of the ligand, Na_2L, in acetonitrile under an argon blanketing atmosphere in the presence of 2 equiv of $Li[B(C_2H_5)_3H]$ and 2 equiv of $[N(n\text{-}Bu)_4]I$ afforded pale orange crystals of $[N(n\text{-}Bu)_4]_2[Cr^{II}L_2]\cdot 4CH_3CN$ (**1**) in 78% yield. The presence of superhydride provides the necessary reducing environment crucial for the slow generation of crystals of **1** where oxygen might slowly diffuse into the reaction vessel.

When a CH_2Cl_2 solution of **1** was exposed to the air, an instantaneous color change to purple was observed. Removal of the solvent in vacuo and recrystallization of the crude solid produced purple crystals of $[N(n\text{-}Bu)_4][Cr^{V}OL_2]\cdot 2CH_2Cl_2$ (**2**) in 93% yield.

The reaction of Na_2L (0.5 equiv), $Co^{II}(CH_3CO_2)_2\cdot 4H_2O$ (0.25 equiv), and $[N(n\text{-}Bu)_4]I$ (0.4 equiv) in methanol at 20 °C in the presence of air produced a deep blue solution. After removal of the solvent in vacuo and recrystallization of the deep blue solid residue from acetonitrile, deep blue crystals of $[N(n\text{-}Bu)_4][CoL_2]$ (**3**) were obtained in 94% yield.

Finally, the reaction of the ligand Na_2L (1.0 equiv) and $[Rh_2(CH_3CN)_{10}](BF_4)_4$ (0.25 equiv) and $[N(n\text{-}Bu)_4]I$ (2 equiv) in acetonitrile under strictly anaerobic conditions at 20 °C afforded a red-brown solution, from which rodlike crystals of $[N(n\text{-}Bu)_4]_2[Rh^{II}L_2]\cdot 4CH_3CN$ (**4**) grew within 3−4 days at −30 °C in 67% yield. The compound is very air-sensitive.

(17) van Lenthe, E.; van der Avoird, A.; Wormer, P. E. S. *J. Chem. Phys.* **1998**, *108*, 4783.
(18) Neese, F.; Olbrich, G. *Chem. Phys. Lett.* **2002**, *362*, 170.

Table 2. Selected Bond Distances (Å) in Complexes **1**−**4**

		complex **1**	
Cr(1)−S(1)	2.365(1)	S(4)−C(8)	1.770(4)
Cr(1)−S(2)	2.359(1)	C(1)−C(2)	1.416(5)
Cr(1)−S(3)	2.368(1)	C(2)−C(3)	1.409(5)
Cr(1)−S(4)	2.365(1)	C(3)−C(4)	1.391(5)
S(1)−C(1)	1.764(4)	C(4)−C(5)	1.403(5)
S(2)−C(2)	1.771(4)	C(5)−C(6)	1.416(5)
S(3)−C(7)	1.781(3)	C(6)−C(1)	1.418(5)
		complex **2**	
Cr(1)−S(1)	2.2781(7)	C(2)−C(3)	1.411(3)
Cr(1)−S(2)	2.2872(7)	C(3)−C(4)	1.400(3)
Cr(1)−S(3)	2.2768(7)	C(4)−C(5)	1.397(3)
Cr(1)−S(4)	2.2803(7)	C(5)−C(6)	1.390(3)
Cr(1)−O(1)	1.585(1)	C(6)−C(1)	1.412(3)
S(1)−C(1)	1.759(2)	C(6)−C(7)	1.411(3)
S(2)−C(2)	1.766(2)	C(7)−C(8)	1.420(3)
S(3)−C(7)	1.771(2)	C(8)−C(9)	1.391(3)
S(4)−C(8)	1.770(2)	C(9)−C(10)	1.396(3)
C(1)−C(2)	1.413(3)	C(10)−C(11)	1.393(3)
		C(11)−C(12)	1.419(3)
complex	**3**	**4**	
M(1)-S(1)	2.1662(6)	2.2715(4)	
M(1)-S(2)	2.1694(6)	2.2701(4)	
S(1)−C(1)	1.772(2)	1.755(1)	
S(2)−C(2)	1.773(2)	1.753(1)	
C(1)−C(2)	1.408(3)	1.414(2)	
C(2)−C(3)	1.416(3)	1.418(2)	
C(3)−C(4)	1.402(3)	1.393(2)	
C(4)−C(5)	1.395(4)	1.396(3)	
C(5)−C(6)	1.404(3)	1.396(2)	
C(6)−C(1)	1.424(3)	1.417(2)	

2. Crystal Structure Determinations. The structures of complexes **1**−**4** have been determined by single-crystal X-ray crystallography at 100(2) K. Crystallographic details are summarized in Table 1, and selected bond distances are given in Table 2. Figure 1 displays the structure of the dianion in **1**, the monoanion in **3**, and the dianion in **4**. Figure 2 exhibits the structure of the monoanion in **2**.

The geometry of the CrS_4 unit in the dianion in **1** is found to be square planar. Despite the fact that four

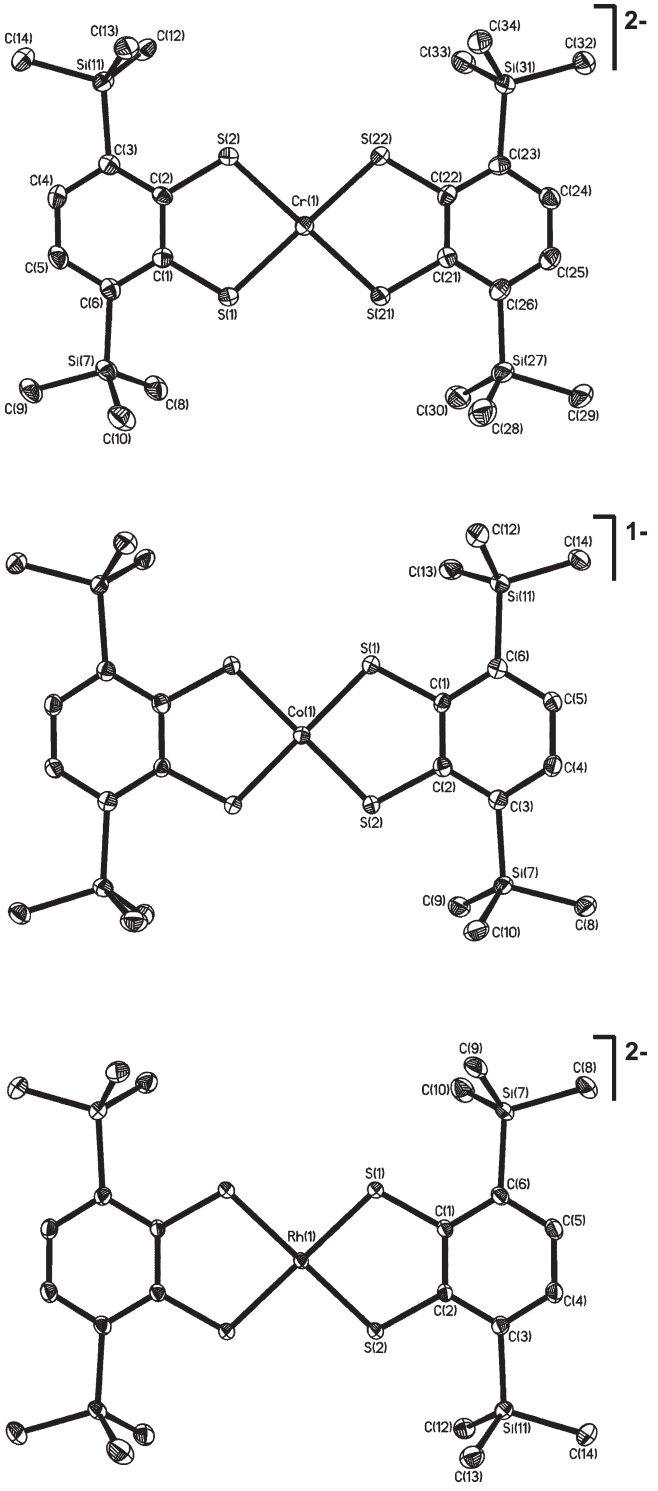

Figure 1. Structure of the dianion $[Cr^{II}L_2]^{2-}$ in crystals of **1** (top), of the monoanion $[Co^{III}L_2]^{-}$ in **3** (middle), and of the dianion $[Rh^{II}L_2]^{2-}$ in **4** (bottom). (Thermal ellipsoids are drawn at the 50% level; hydrogen atoms are omitted.)

molecules of acetonitrile per formula unit are present, none of these molecules is coordinated to the central chromium(II) ion. Thus, the metal ion is in a four-coordinate, square-planar environment of four sulfur donor atoms. The average C−S distance at 1.772 ± 0.01 Å is long and indicates the presence of two closed-shell dithiolate ligands, rendering the oxidation state of the

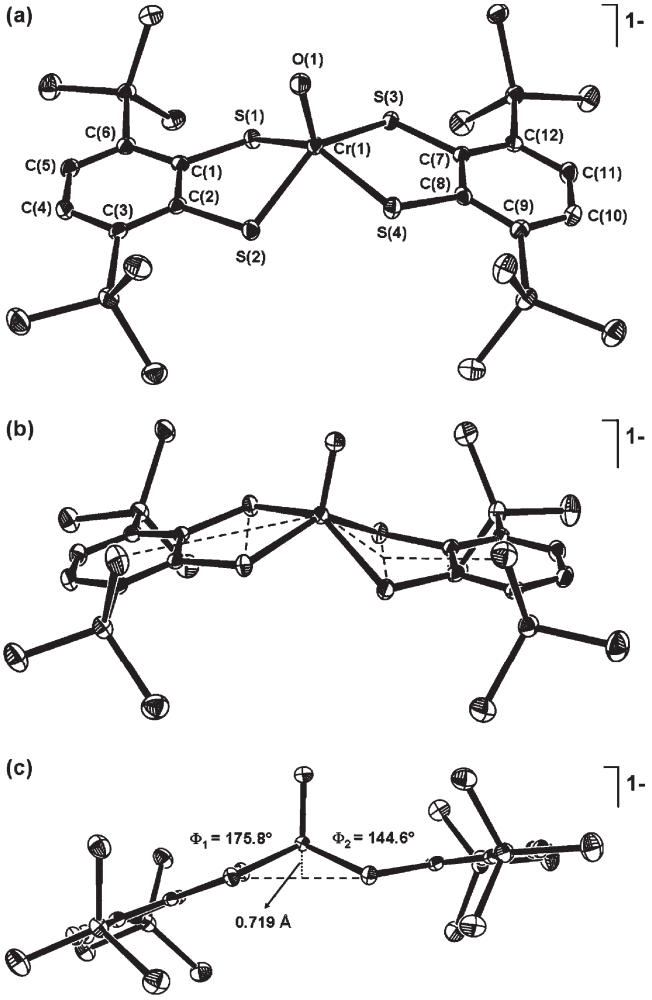

Figure 2. (a) Structure of the monoanion $[Cr^{V}OL_2]^{-}$ in crystals of **2**; (b) definition of the two folding angles ϕ_1 and ϕ_2; (c) view of the anion perpendicular to the Cr−O vector.

central chromium ion +II (d^4). The average C−C distance at 1.408 ± 0.01 Å indicates the presence of an aromatic benzene ring. The average Cr−S distance at 2.364 ± 0.003 Å is identical to that reported by Sellmann et al.[3] for $[Cr^{II}(bdt)_2]^{2-}$ (bdt = benzene-1,2-dithiolate(2−)) and slightly shorter than that reported for $[Cr^{II}(edt)_2]^{2-}$ at 2.388 Å.[2]

The monoanion in crystals of **2** possesses an approximately square-pyramidal $CrOS_4$ polyhedron where four sulfur donor atoms occupy the equatorial positions and the terminal oxo ligand is in the apical position. Overall, the structure is very similar to that reported recently by us[19] for $[Cr^{V}O(L^{Bu})_2]^{-}$ (L^{Bu} = 3,5-di-*tert*-butyl-1,2-benzenedithiolate(2−)). The Cr−O bond is short at 1.585(1) Å and indicates a double bond. An interesting feature is the dihedral angle ϕ between the mean S−C−C−S trapezoidal ligand plane and the S−Cr−S plane, which results in a folding of the five-membered (dithiolato)chromium chelate ring about the S···S vector. The extent of this folding is different for each of the two ligands (ϕ_1 = 175.8°, ϕ_2 = 144.6°). The difference $\phi_1 - \phi_2$ is 31°; it is ∼20° for $[CrO(L^{Bu})_2]^{-}$ and $[CrO(L^{Me})_2]^{-}$

(19) Kapre, R.; Ray, K.; Sylvestre, I.; Weyhermüller, T.; DeBeer George, S.; Neese, F.; Wieghardt, K. *Inorg. Chem.* **2006**, *45*, 3499.

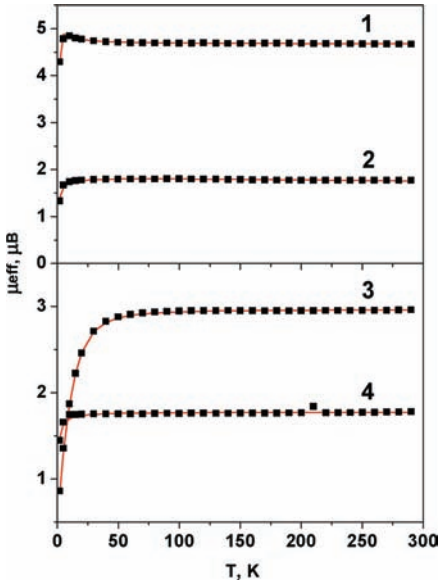

Figure 3. Temperature dependence of magnetic moments of solid samples of **1**, **2**, **3**, and **4** in an applied field of 1 T. The experimental data were fitted (red line) by using the following parameters: (**1**) $S = 2$; $g = 1.96$; Weiss constant $\theta = 1.0$ K; $|D| = 2.2$ cm^{-1}; $\chi_{TIP} = 106 \times 10^{-6}$ emu; (**2**) $S = {}^1/_2$; $g = 1.998$; $\theta = -2.1$ K; $\chi_{TIP} = 351 \times 10^{-6}$ emu; (**3**) $S = 1$; $g = 2.094$; $|D| = 35$ cm^{-1}; (**4**) $S = {}^1/_2$; $g = 2.046$; $\theta = -0.8$ K; $\chi_{TIP} = 646 \times 10^{-6}$ emu.

(L^{Me} = toluene-1,2-dithiolate(2−)).[19] It has been shown by DFT calculations on the latter two complexes that the difference is electronic in origin (not steric) and has been attributed to strong S(3p) → Cr($3d_{x^2-y^2}$) π-donation providing, thereby, additional stability to the complexes. The same holds true for **2** (see below). Interestingly, the average Cr−S distance in **2** at 2.280 ± 0.002 Å is significantly shorter than in **1** despite an increased coordination number, which is 5 in **2** but 4 in **1**. We take this as a clear indication that the oxidation state in **2** is +V (d^1) but +II (d^4) in **1**. The C−S and C−C bond lengths in **2** are, within experimental error, the same as in **1**, indicating the presence of two closed-shell dithiolate(2−) ligands.

The geometries of the CoS_4 and RhS_4 units in **3** and **4** are again strictly square planar. None of the solvent acetonitrile molecules in **4** are coordinated to the central Rh^{II} ion. The metrical details of the two *S*,*S*′-coordinated dithiolate ligands L^{2-} in each species are very similar and indicate the presence of closed-shell ligand dianions. The oxidation state of the central metal ion is therefore +III in **3** and +II in **4**. We note that **4** represents the first crystal structure of a bis(dithiolene)rhodium complex.[1]

The structure of square planar $[Co(L)_2]^-$ is very similar to that of $[Co(L^{Bu})_2]^-$ reported in ref [20b] and resembles closely in all parameters the structure of $[Co(tdt)_2]^-$ ($(tdt)^{2-}$ = toluene-3,4-dithiolato) in ref [20a], which was reported in 1968.

3. Magnetic Properties and EPR Spectra. Figure 3 displays the temperature dependence of magnetic moments of **1**−**4**. From measurements of the molar magnetic susceptibility of a powdered sample of **1** in an applied field of 1.0 T and a temperature range 2−296 K, a temperature-independent magnetic moment of 4.69 ± 0.01 μ_B has been established, which indicates an $S = 2$ ground state (high-spin Cr(II), d^4).

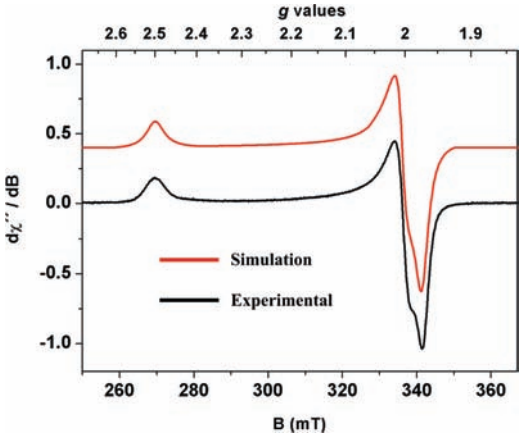

Figure 4. X-band EPR spectrum of a frozen CH_2Cl_2 solution of **4** at 25 K. (Conditions: frequency, 9.43 GHz; modulation, 5 G; power, 2.007 × 10^{-4} W.) Simulation parameters (red line): $g_1 = 2.500$; $g_2 = 2.005$; $g_3 = 1.974$; line widths, $W_x = 5.02$ mT, $W_y = 4.69$ mT, $W_z = 6.71$ mT.

Similarly, for **2**, a temperature-independent (20−300 K) magnetic moment of 1.77 μ_B indicates the presence of a single unpaired electron ($S = {}^1/_2$) typical for a Cr(V) (d^1) ion. Its X-band EPR spectrum (Figure S1, Supporting Information) in frozen CH_2Cl_2 at 10 K displays a rhombic signal with $g_1 = 2.023$, $g_2 = 1.997$, and $g_3 = 1.987$ ($g_{iso} = 2.002$) without resolved hyperfine coupling to ^{53}Cr ($I = {}^3/_2$; 10% natural abundance). These data are quite typical for Cr(V) oxo complexes with four sulfur donor ligands.[19,21]

Figure 3 shows the magnetic behavior of solid, powdered **3** in the temperature range 2−290 K and an applied field of 1.0 T. Above 50 K, a temperature-independent magnetic moment of 2.84 ± 0.01 μ_B is observed, indicating the presence of two unpaired electrons ($S = 1$ ground state). The monotonic decrease of μ_{eff} below 70 K has been successfully modeled by taking into account a large zero-field splitting of $|D| = 35$ cm^{-1} ($g = 2.09$). Very similar behavior has been reported[9] for $[Co(L^{Bu})_2]^-$ ($D = +32$ cm^{-1}), where the positive sign of D has been experimentally established. The physical origin of this large zero-field splitting has been found to be due to the presence of low-energy, spin-conserved d−d excitations, which lead to a large anisotropic D_{zz} through efficient spin−orbit coupling.[20]

Figure 3 (bottom) displays the temperature dependence of the magnetic moment of a solid, powdered sample of **4**. A temperature-independent (10−300 K) μ_{eff} of 1.77 ± 0.05 indicates an $S = {}^1/_2$ ground state (Rh^{II}, low-spin d^7). This is nicely corroborated by its X-band EPR spectrum recorded in frozen CH_2Cl_2 at 25 K (Figure 4). From the simulation, the following parameters are deduced: $g_1 = 2.500$, $g_2 = 2.005$, and $g_3 = 1.974$. These values agree nicely with those reported by Holm et al.[5] for $[N(n\text{-}Bu)_4]_2[Rh(mnt)_2]$ ($g_1 = 2.447$, $g_2 = 2.019$, and $g_3 = 1.936$) doped in diamagnetic $[N(n\text{-}Bu)_4]_2[Ni^{II}(mnt)_2]$, where mnt^{2-} represents 1,2-maleonitrile-1,2-dithiolate(2−). The spectrum

(20) (a) Eisenberg, R.; Dori, Z.; Gray, H. B.; Ibers, J. A. *Inorg. Chem.* **1968**, *7*, 741. (b) Ray, K.; Begum, A.; Weyhermüller, T.; Piligkos, S.; van Slageren, J.; Neese, F.; Wieghardt, K. *J. Am. Chem. Soc.* **2005**, *127*, 4403.
(21) (a) Levina, A.; Zhang, L.; Lay, P. A. *Inorg. Chem.* **2003**, *42*, 767. (b) Stiefel, E. I.; Eisenberg, R.; Rosenberg, R. C.; Gray, H. B. *J. Am. Chem. Soc.* **1966**, *88*, 2956.

Table 3. Redox Potentials of Complexes **1**−**4** in CH_2Cl_2 Solutions (0.10 M $[N(n\text{-}Bu)_4]PF_6$; 25 °C; glassy carbon working electrode; scan rate = 100 mV s^{-1}) Referenced versus the Fc^+/Fc Couple[a]

complex	$E^1_{1/2}$, V	$E^2_{1/2}$, V	ref
1	−1.05 r	−1.31 r	this work
2	+0.12 r	−1.05 r	this work
$[Cr^VO(L^{Bu})_2]^-$	+0.15 qr	−0.96 r	19
$[Cr^VO(L^{Me})_2]^-$	+0.16 qr	−0.96 r	19
3	−0.48 irr	−1.40 r	this work
	−0.07 irr		
4	−0.36 irr	−1.21 r	this work

[a] r = reversible; qr = quasi-reversible; irr = irreversible.

of a polycrystalline sample of $[N(n\text{-}Bu)_4][Rh(mnt)_2]$ reported by Gray et al.[4] displays slightly different parameters ($g_1 = 2.35$, $g_2 = 2.02$, and $g_3 = 1.95$). The relatively large observed **g** anisotropy for **4** is taken as evidence that the unpaired electron resides in an orbital with significant 4d metal character.

In fact, the **g** values of **4** can be rationalized by a ligand field approach based on the electron configuration obtained from DFT calculations (see below). The orbital splitting diagram for a $4d^7$ configuration with a $^2B_1$ ground state in C_{2v} symmetry is shown in Figure S2 (Supporting Information) in conjunction with a generic sequence of excited states and the assignment of their energies relative to the ground state.

A perturbation treatment of the Zeeman splitting of the ground state yields diagonal elements of the **g** matrix according to the relations 1−3

$$g_x \sim 2.0023 + 6(\zeta_{n,d}/\Delta_3) + 2(\zeta_{n,d}/\Delta_4) + \quad (1)$$

$$g_y \sim 2.0023 - 2(\zeta_{n,d}/\Delta_2) + \quad ... \quad (2)$$

$$g_z \sim 2.0023 - 2(\zeta_{n,d}/\Delta_1) + \quad ... \quad (3)$$

in which terms of the order $(\zeta_{n,d}/\Delta_i)^2$ as well as mixing of $|x^2 - y^2|\rangle$ and $|z^2\rangle$ d orbitals (allowed in D_{2h} symmetry) have been neglected. Here, $\zeta_{n,d}$ is the single-electron spin−orbit coupling constant for a $4d^7$ configuration.

Assuming $(\zeta_{n,d}/\Delta_i)$ to be sufficiently small such that the perturbation approach is valid, the equations indicate $g_y \approx g_z < 2$ and $g_x > 2$, consistent with the experimental data. This clearly supports the assignment of a $^2B_{2g}$ ground state for **4** with a $(x^2-y^2)^2(z^2)^2(yz)^2(xz)^1$ configuration, in contrast to the alternative of a $^2A_{1g}$ ground state with $(x^2-y^2)^2(z^2)^1(yz)^2(xz)^2$ configuration having the electron in the $|z^2\rangle$ orbital. In that case, the **g** values usually show a splitting pattern, $g_z \approx 2$ and $g_x \approx g_y > 2$.

4. Eletro- and Spectroelectrochemistry. Cyclic voltammograms (CV) of complexes **1**, **2**, **3**, and **4** have been recorded at 25 °C in CH_2Cl_2 solutions containing a 0.1 M $[N(n\text{-}Bu)_4]PF_6$ supporting electrolyte and ~1 mmol of the complex. The redox potentials are referenced versus the ferrocenium/ferrocene (Fc^+/Fc) couple (ferrocene internal standard). Table 3 summarizes the results.

The CV of **1** (Figure 5 (top)) displays two reversible electron transfer waves at rather low potentials.

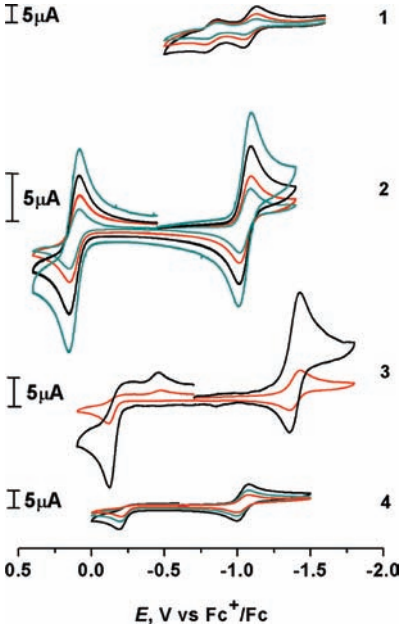

Figure 5. (a) Cyclic voltammogram of **1** in CH_2Cl_2 solution at 25 °C (0.1 M $[N(n\text{-}Bu)_4]PF_6$) recorded at scan rates 50 (blue line), 100 (red), and 200 (black) mV s^{-1} (glassy carbon working electrode). (b) CV of **2** in CH_2Cl_2 solution (0.1 M $[N(n\text{-}Bu)_4]PF_6$) at 25 °C at scan rates of 400 (blue), 200 (black), 100 (red), and 50 mV s^{-1} (green). (c) CV of **3** (CH_2Cl_2); 0.1 M $[N(n\text{-}Bu)_4]PF_6$; scan rate, 100 mV s^{-1}. (d) CV of **4** (CH_2Cl_2); 0.1 M $[N(n\text{Bu})_4]PF_6$; scan rate, 50 (red), 100 (blue); and 200 (black) mV s^{-1}. The CVs were recorded as cathodic scans.

Due to the instability and enormous oxygen sensitivity of the above solutions, the nature of these one-electron processes could not be investigated in further detail.

In contrast, the CV of **2** (Figure 5) is very well behaved. Two fully reversible one-electron transfer waves are observed. Coulometric experiments established that **2** can be one-electron reduced at very low potentials and one-electron oxidized at positive potentials versus Fc^+/Fc, as denoted in eq 4.

$$[Cr^{IV}O(L)_2]^{2-} \underset{-e}{\overset{+e}{\rightleftharpoons}} [Cr^{V}O(L)_2]^{1-} \underset{-e}{\overset{+e}{\rightleftharpoons}} [Cr^{VI}O(L)_2]^{0} \quad (4)$$

The electrochemistry of $[Cr^VO(L^{Bu})_2]^-$ and $[Cr^VO(L^{Me})_2]^-$ is very similar.[19] Thus, the redox chemistry of **2** involves a metal-centered reduction, affording an (oxo)Cr(IV) species and a metal-centered oxidation yielding an (oxo)chromium(VI) species. On the time scale of coulometric experiments (>5 min), solutions of $[Cr^{VI}O(L)_2]^0$ are not stable, whereas the reduced dianion, although air-sensitive, is remarkably stable. Therefore, it has been possible to record the electronic spectrum of the latter, as shown in Figure 6.

The CV of **3** (Figure 5) exhibits a fully reversible one-electron reduction wave at −1.40 V and an irreversible oxidation at a peak potential $E_{p,ox}$ of ~0.07 V. Upon rereduction, a peak $E_{p,red}$ at −0.48 V is observed. Spectroelectrochemically, both processes (the one-electron oxidation and the one-electron reduction of $[Co(L)_2]^-$) were followed as shown in Figure 7 (top and bottom) and summarized in Table 4. Interestingly, the spectral changes observed during the coulometric one-electron oxidation

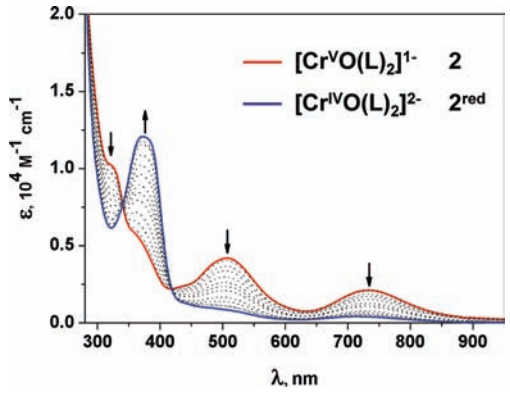

Figure 6. Spectral changes observed during the electrochemical reduction of **2** (red line) affording $[Cr^{IV}O(L)_2]^{2-}$ (blue line) in CH_2Cl_2 solution (0.1 M $[N(n\text{-}Bu)_4]PF_6$).

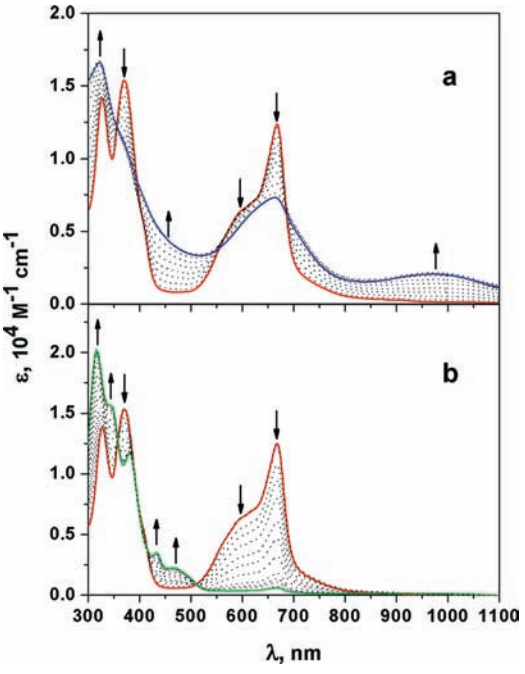

Figure 7. Spectral changes observed during the electrochemical one-electron oxidation of **3** in CH_2Cl_2 (0.1 M $[N(n\text{-}Bu)_4]PF_6$ at 25 °C. The line in red represents the spectrum of **3** and, in blue, that of the final, EPR-silent, one-electron oxidized form. Bottom: Spectral changes during one-electron reduction of **3** (red, spectrum of **3**; green, that of $[Co^{II}L_2]^{2-}$.

display four well-defined isosbestic points at 360, 400, 550, and 690 nm. One-electron oxidation of **3** does not lead to decomposition products since, after completion of this one-electron oxidation as judged by coulometry, the same CV as in Figure 7 can be recorded.

This demonstrates that the oxidized neutral form undergoes a (slow) reversible chemical reaction. Since the oxidized solution is EPR-silent, we propose a simple dimerization affording $[Co^{III}(L)(L^{\bullet})]_2$, $(\mathbf{3}^{ox})_2$, where $L^{\bullet}$ is the monoanionic ligand π radical. We do not know the exact structure of this dimer, but it could involve S−S bond formation between two S-centered radicals. The two CoS_4 planes need not be coplanar (sterically not possible) but could be perpendicular relative to each other, which is sterically not encumbered.

Thus, we propose the following redox scheme for **3** shown in eq 5.

$$\underset{S=1/2}{[Co^{III}(L)(L^{\bullet})]^0} \underset{+e}{\overset{-e}{\rightleftharpoons}} \underset{S=1}{[Co^{III}(L)_2]^{1-}} \underset{+e}{\overset{-e}{\rightleftharpoons}} \underset{S=1/2}{[Co^{II}(L)_2]^{2-}}$$

$$\text{slow} \leftrightarrows \text{fast} \; \underset{S=0}{[Co^{III}(L)(L^{\bullet})]_2} \qquad (5)$$

The presence of *S*,*S*′-coordinated $(L^{\bullet})^-$ π radicals has been established by EPR spectroscopy in the following fashion. To a ~1 mmol solution of **3** in CH_2Cl_2 was added 1 equiv of ferrocenium hexafluorophosphate at 25 °C. After rapid dissolution of the salt, the solution was rapidly frozen in liquid nitrogen in an EPR test tube (77 K) in order to avoid complete dimerization of the chemically generated monomeric radical $[Co^{III}(L)(L^{\bullet})]^0$. The then-recorded X-band EPR spectrum of this solution at 10 K is shown in Figure 8. Gratifyingly, it confirms the presence of an $S = {}^1/_2$ species, which shows hyperfine coupling with the ^{59}Co ($I = {}^7/_2$, 100%) nucleus. The satisfactory simulation yielded parameters $g_1 = 2.050$, $g_2 = 2.032$, and $g_3 = 2.005$ and $A_1 = 7.3 \times 10^{-4}$ cm^{-1}, $A_2 = 54.50 \times 10^{-4}$ cm^{-1}, and $A_3 = -1.33 \times 10^{-4}$ cm^{-1}, with $g_{iso} = 2.023$ and $A_{iso} = 21.0 \times 10^{-4}$ cm^{-1}.

The spectrum resembles closely that reported for an octahedral Co(III) (d^6, $S_{Co} = 0$) complex S-coordinated to a thiyl (sulfur centered) π radical:[22] $g_{iso} = 2.022$ and ^{59}Co-$A_{iso} = 10.7 \times 10^{-4}$ cm^{-1}. The relatively small ^{59}Co hyperfine coupling constant indicates the presence of a sulfur-centered radical S-coordinated to a diamagnetic, low-spin Co(III) ion. Thus, the chemically one-electron oxidized species $[Co^{III}(L)(L^{\bullet})]^0$ presumably added two adventitiously present water molecules, generating the octahedral species $[Co^{III}(L)(L^{\bullet})(H_2O)_2]^0$, eq 6:

$$\underset{S_{Co}=1}{[Co^{III}(L)_2]^-} + Fc^+ \rightarrow \underset{S_{Co}=1;S_{L\bullet}=1/2;S_t=1/2}{[Co^{III}(L)(L^{\bullet})]^0} +$$

$$Fc \xrightarrow{H_2O} \underset{S_{Co}=0;S_{L\bullet}=1/2;S_t=1/2}{[Co(L)(L^{\bullet})(H_2O)_2]^0} \qquad (6)$$

which contains low-spin Co(III) ions (d^6; $S_{Co} = 0$) and a ligand π radical $(L^{\bullet})^-$ ($S_{rad} = {}^1/_2$).

The CV of **4** in CH_2Cl_2 solution exhibits a fully reversible one-electron reduction wave at −1.21 V and an irreversible oxidation at a peak potential of −0.36 V (Figure 5; Table 3), eq 7.

$$\underset{(?)}{[Rh(L)_2]^{1-}} \underset{-e}{\leftarrow} \underset{S=1/2}{[Rh^{II}(L)_2]^{2-}} \underset{+e}{\overset{-e}{\rightleftharpoons}} \underset{S=0}{[Rh^{I}(L)_2]^{3-}} \qquad (7)$$

Changes in the electronic spectrum upon electrochemical reduction of **4** by one electron are displayed in Figure 9 and summarized in Table 4. It is remarkable that the

(22) Kimura, S.; Bill, E.; Bothe, E.; Weyhermüller, T.; Wieghardt, K. *J. Am. Chem. Soc.* **2001**, *123*, 6025.

Table 4. Electronic Spectra of Complexes in CH_2Cl_2 Solution at 25 °C

complex	λ_{max}, nm (ε, M^{-1} cm^{-1})
1	471(82)
2	322(1.0×10^4), 363(0.6×10^4), 506(0.4×10^4), 732(0.2×10^4)
$\mathbf{2}^{red\ a}$	371(1.2×10^4)
3	328(1.4×10^4), 370(1.5×10^4), 534sh(0.3×10^4), 594sh(0.6×10^4), 630(0.7×10^4), 668(1.3×10^4)
$\mathbf{3}^{ox\ a}$	324(1.7×10^4), 367sh(1.7×10^4), 661(0.7×10^4), 981(0.2×10^4)
$\mathbf{3}^{red\ a}$	316(2.0×10^4), 342(1.6×10^4), 381(1.2×10^4), 433(0.4×10^4), 470(0.2×10^4)
4	388(1.2×10^4), 500(0.2×10^4), 752(2.3×10^4)
$\mathbf{4}^{red\ a}$	352(1.1×10^4), 383(1.0×10^4), 493(0.4×10^4), 609(0.6×10^4), 753(1.2×10^4)

[a] Generated electrochemically in CH_2Cl_2 solution containing 0.10 M $[N(n\text{-}Bu)_4]PF_6$.

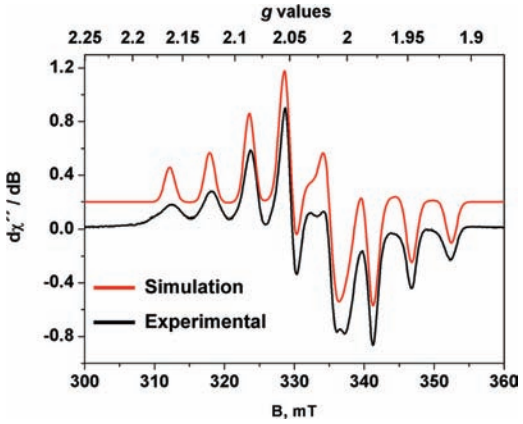

Figure 8. X-band EPR spectrum of a chemically (ferrocenium) one-electron oxidized CH_2Cl_2 solution of **3** recorded at 10 K. (Conditions: frequency, 9.45 GHz; modulation, 1 G; power, 2.5×10^{-6} mW.) Simulation parameters: $S = {}^1/_2$; $g_1 = 2.050$; $g_2 = 2.032$; $g_3 = 2.005$. Line widths, $W_x = 5.02$ mT, $W_y = 4.69$ mT, $W_z = 6.71$ mT. ^{59}Co hyperfine coupling constants in 10^{-4} cm^{-1}: $A_1 = 7.31$, $A_2 = 54.50$, $A_3 = -1.33$. The black line represents the experimental spectrum, and the red is the simulation.

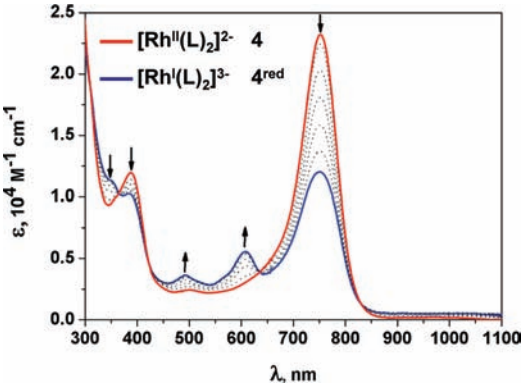

Figure 9. Spectral changes observed during the electrochemical one-electron reduction of **4** (red line) affording the trianion $[Rh^I(L)_2]^{3-}$ (blue line) in CH_2Cl_2 solution (25 °C; 0.1 M $[N(n\text{-}Bu)_4]PF_6$).

intense absorption maximum of **4** at 752 nm ($\varepsilon \approx 2.3 \times 10^4$ M^{-1} cm^{-1}) is still present in the spectrum of the trianion $[Rh^I(L)_2]^{3-}$ but with reduced intensity ($\varepsilon = 1.2 \times 10^4$ M^{-1} cm^{-1}). We will tentatively assign the intense transitions by time-dependent density functional calculations of the two spectra as a $1b_{1u} \rightarrow 2b_{2g}$ transition (ligand-to-metal charge transfer (LMCT) yielding a $^3B_{2u}$ excited state), whereas for the Rh^I species this band is due to a $2b_{2g} \rightarrow 2b_{1u}$ transition (HOMO → LUMO), which is essentially a metal-to-ligand transition.

5. Preliminary Reactivity Study of $[Rh^IL_2]^{3-}$. Attempts to isolate a salt containing the trianion $[Rh^IL_2]^{3-}$ were not successful. The reaction of **4** with Na/Hg amalgam in dry acetonitrile afforded a violet solution containing the diamagnetic trianion $[Rh^IL_2]^{3-}$. The electronic absorption spectrum of this solution is very similar to that reported above for the electrochemically one-electron reduced form of **4**. To such a violet solution, a 4−5-fold excess of CH_3I was added, initiating a rapid color change to orange at room temperature. Slow evaporation of the solvent gave orange crystals suitable for X-ray crystallography in ~80% yield. The X-ray structure determination revealed that two different neutral, octahedral complexes cocrystallized: *cis*-$[Rh^{III}I_2(L')(L'')]$ (70%) and *cis*-$[Rh^{III}(CH_3)I(L'')(L')]$ (30%). [The crystal structure determination at 100(2) K with Mo Kα radiation yielded the following crystallographic parameters: monoclinic space group, $P2_1/c$ (No. 14); $a = 13.0640(4)$, $b = 20.3985(6)$, $c = 14.6090(4)$ Å, $\beta = 99.387(3)°$; $V = 3841.0(2)$ Å^3. The structure consists of two different octahedral, neutral complexes (ratio 70:30) (see text) which are statically disordered. They were successfully refined with split atom positions yielding final residuals $R_1 = 0.031$, GOF = 1.104, and wR_2 (all data) = 0.063. Full crystallographic data including atom coordinates, bond distances, and angles and figures of both cocrystallization products are given in the Supporting Information. We have ascertained the reproducibility of the formation of these crystals three times. The structure determination unambiguously established the atom connectivity of the two neutral species (and their ratio in the solid state).] Attempts to separate the two complexes by liquid chromatography with differing stationary and mobile phases were unsuccessful; no separation of species was achieved on silica gel or alumina columns (eluent 1:1 CH_3CN/CH_2Cl_2 or pure CH_3CN or CH_2Cl_2).

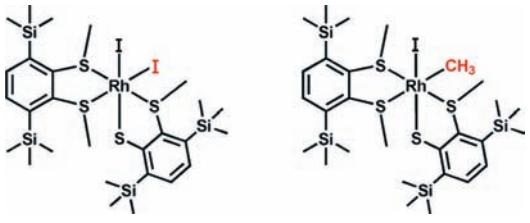

Interestingly, three of the four sulfur donor atoms in $[Rh^IL_2]^{3-}$ are now methylated by CH_3I, yielding neutral

Table 5. Experimental and Calculated (in parentheses) Metrical Parameters (in Å) of Complexes

complex	M-S	C−S	C1−C2	C2−C3	C3−C4	C4−C5	C5−C6	C6−C1
1	2.364	1.776	1.416	1.409	1.391	1.403	1.416	1.418
	(2.404)	(1.771)	(1.418)	(1.416)	(1.403)	(1.391)	(1.409)	(1.410)
3	2.166	1.772	1.408	1.416	1.402	1.395	1.404	1.424
	(2.213)	(1.781)	(1.416)	(1.408)	(1.406)	(1.398)	(1.406)	(1.421)
$[\mathbf{3}^{Red}]^{2-}$								
	(2.234)	(1.782)	(1.426)	(1.424)	(1.408)	(1.400)	(1.408)	(1.423)
4	2.271	1.755	1.414	1.418	1.393	1.396	1.396	1.417
	(2.296)	(1.768)	(1.431)	(1.423)	(1.407)	(1.403)	(1.407)	(1.423)
$[\mathbf{4}^{Red}]^{3-}$								
	(2.307)	(1.781)	(1.434)	(1.424)	(1.413)	(1.401)	(1.413)	(1.424)

L″ and monoanionic $(L')^-$, probably via simple S_N2 substitution reactions. Similar chemistry has been reported for $[Ni^{II}(pdt)_2]^{2-}$ reacting with CH_3I, where a product *trans*-$[Ni^{II}I_2(Ph_2C_2S_2Me_2)_2]$ has been identified.[23] The Rh^I center then undergoes a classic oxidative addition reaction with CH_3I, as has been described for the reaction of $[(OETAP)Rh]_2$ with CH_3I, affording exclusively $[(OETAP)Rh^{III}I]^0$ and $[(OETAP)Rh^{III}(CH_3)]^0$ in a 1:1 ratio.[24] $(OETAP)^{2-}$ represents the octaethyltetraazaporphyrinate dianion.

6. Calculations. The geometry optimizations were carried out at the B3LYP level of DFT. The property calculations at optimized geometries were also done with the B3LYP functional.

7. Optimized Geometries. Table 5 summarizes selected experimental and calculated bond lengths of the square planar mono-, di-, and trianions $[CoL_2]^{-/2-}$, $[RhL_2]^{2-/3-}$, and $[CrL_2]^{2-}$. In general, the calculated geometries are in very good agreement with experimental data (where available). Deviations of M−S, C−S, and C−C bond lengths from experimental results do not exceed ±0.03 Å. For all complexes, the C−S bonds are long (1.76−1.78 Å), indicating the presence of closed-shell, *S*,*S*′-coordinated dianions L^{2-} and the absence of π radical character in these ligands. The calculated geometry and metrical parameters for the monoanion in **2** are also found to be in very good agreement with experimental values (Table S6, Supporting Information). As has been shown for $[CrO(bdt)_2]^-$ in ref 19, the approximate square-based pyramidal geometry is well-reproduced in the calculation. Even the symmetry lowering from C_{2v} to C_s due to the folding of the C−S−S−C trapezoid along the S···S vector on either side of the Cr atom is observed. The calculated dihedral angles for **2**, $\phi_1 = 142.0°$ and $\phi_2 = 175.9°$, agree nicely with experimental results (144.6° and 175.8°), which indicates an electronic origin of this folding, as explained above and in ref 19 in detail. The presence of the terminal oxo donor results in the metal residing ~0.72 Å (calculated 0.72 Å) out of the bis(dithiolate) S_4 plane.

8. Bonding Schemes. For the MO description of the square planar complexes within the D_{2h} point group, we choose the *z* axis to be along the normal of the S_4 plane; the *x* axis is then along the long axis of the complex and *y* axis along the short axis, as shown in Figures 10 and 11,

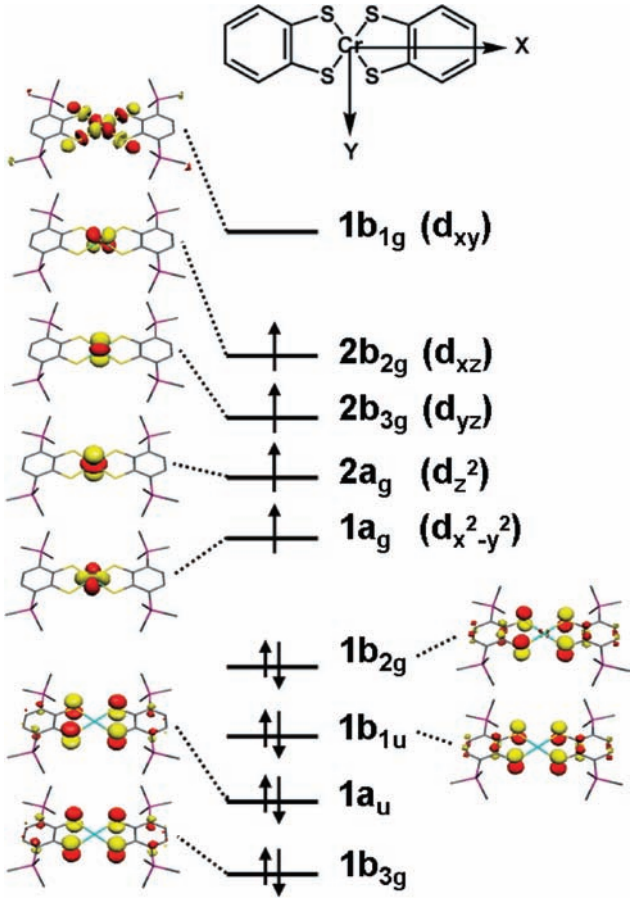

Figure 10. Qualitative MO diagram of **1** displaying Kohn−Sham MOs from a spin-unrestricted ZORA-B3LYP DFT calculation.

where qualitative MO schemes for the dianion in **1** and the $[RhL_2]^{2-/3-}$, respectively, are displayed as a result of an unrestricted ZORA-B3LYP DFT calculation. The ground state electronic configuration of the $[Cr^{II}(bdt)_2]^{2-}$ species is predicted to be $^3B_{1g}$:

$$(1a_u)^2(1b_{3g})^2(1b_{1u})^2(1b_{2g})^2(1a_g)^1(2a_g)^1(2b_{2g})^1$$
$$(2b_{3g})^1(1b_{1g})^0$$

This bonding scheme reveals that four, singly occupied metal d orbitals are highest in energy as compared to the filled ligand-based $1b_{2g}$ and $1b_{3g}$ orbitals, which undergo symmetry-allowed π interactions with the metal d orbitals. The four metal SOMOs are the hallmark of a chromium(II) ion (high-spin d^4), and the one-electron oxidation of **1** is predicted to be a metal-centered process.

In a previous report,[20] we calculated the electronic structure of $[Co(bdt)_2]^-$ with a $^3B_{1g}$ ground state with the following electronic configuration:

$$(1a_g)^2(2a_g)^2(1b_{3g})^2(1a_u)^2(1b_{2g})^2(1b_{1u})^2(2b_{2g})^1$$
$$(2b_{3g})^1(1b_{1g})^0$$

(23) Schrauzer, G. N.; Zhang, C.; Schlemper, E. O. *Inorg. Chem.* **1990**, *29*, 3371.
(24) Ni, Y. N.; Fitzgerald, J. P.; Carroll, P.; Wayland, B. B. *Inorg. Chem.* **1994**, *33*, 2029.
(25) Bill, E.; Bothe, E.; Chaudhuri, P.; Chlopek, K.; Herebian, D.; Kokatam, S.; Ray, K.; Weyhermüller, T.; Neese, F.; Wieghardt, K. *Chem.—Eur. J.* **2005**, *11*, 204.

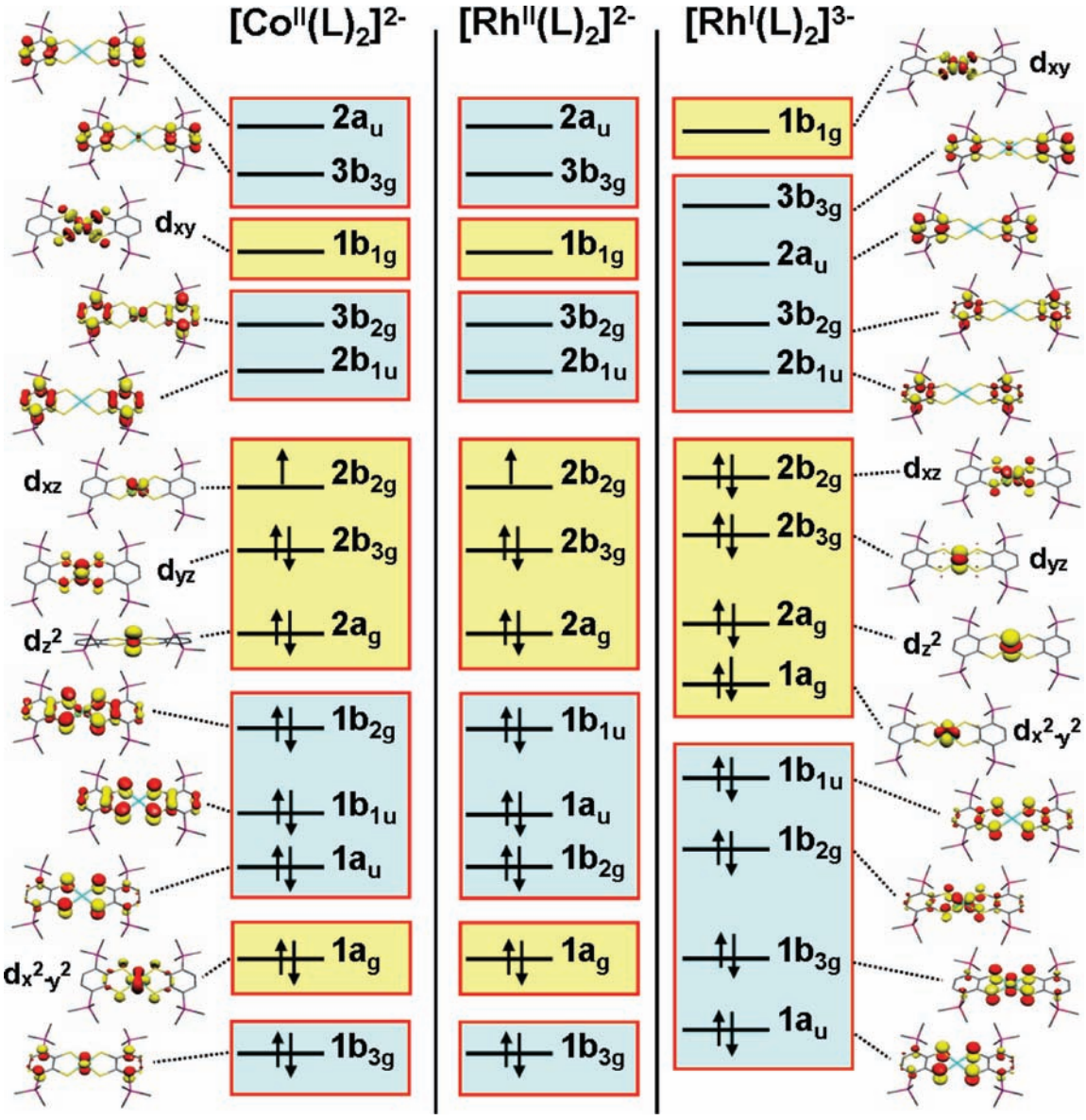

Figure 11. Qualitative MO schemes for $[Co^{II}(L)_2]^{2-}$, $[Rh^{II}(L)_2]^{2-}$, and $[Rh^{I}(L)_2]^{3-}$ from spin-unrestricted ZORA-B3LYP DFT calculations. The yellow shaded regions represent predominantly metal-based orbitals, whereas the blue shaded areas represent ligand-based orbitals.

The same configuration has been deduced for square planar $[Co(^1L_N)_2]^-$, where $(^1L_N)^{2-}$ represents the N,N′-coordinated N-phenyl-*o*-phenylenediamide(2−) ligand[25] and the present complex **3**. The ligand character of the $2b_{2g}$ orbital in **3** is found to be only 29% (Table 3), and therefore, the description of the electronic structure of this monoanionic species **3** as containing an intermediate-spin Co(III) ion *S*,*S*′-coordinated to two dianionic benzene-1,2-dithiolate(2−) ligands is somewhat less ambiguous than in the previous cases. We note that this orbital in **3** has the highest metal character of the series at 71%; it is only 65% for $[Co(bdt)_2]^-$ and 47% for $[Co(^1L_N)_2]^-$. In the corresponding complex $[Co(L^{Red})_2]^-$, where $(L^{Red})^{2-}$ represents the dianionic form of bis(2,6-diisopropylphenyl)glyoxal, the $2b_{2g}$ orbital was found to possess 57% ligand character and only 43% metal character.[26] It is worth mentioning that the *n*d electron distribution in $[Co(bdt)_2]^-$ and **3** *decreases* from 7.8 to 7.6, and the spin density at the cobalt ion *increases* from 1.59 to 1.78. This is a clear indication that the Co(III) (d^6; S = 1) character in **3** is more pronounced than in $[Co(bdt)_2]^{-9}$ (see Table 6).

Table 6. Comparison of the Spin Population at the Metal Ion from a Natural Population Analysis (Scalar Relativistic ZORA-B3LYP DFT Calculations)

complex	electrons-*n*d	electrons (*n* + 1)s	Spin-*n*d	metal oxidation state
1	4.91	0.49	3.89	Cr(II)
3	7.58	0.47	1.78	Co(III), see text
$[\mathbf{3}^{Red}]^{2-}$	8.34	0.46	1.01	Co(II)
4	8.31	0.50	0.66	Rh(II)
$[\mathbf{4}^{Red}]^{3-}$	9.21	0.59	0.00	Rh(I)
$[Fe(bdt)_2]^{2-}$ [a]	7.11	0.49	1.92	Fe(II)
$[Co(bdt)_2]^{-}$ [a]	7.82	0.51	1.59	see text
$[Ni(bdt)_2]^{2-}$ [b]	9.13	0.51	0.00	Ni(II)

[a] Ref 20. [b] Refs 28, 29.

(26) Spikes, G. H.; Milsmann, C.; Bill, E.; Weyhermüller, T.; Wieghardt, K. *Inorg. Chem.* **2008**, *47*, 11745.

Table 7. Composition of Selected Molecular Orbitals of $[M(L)_2]^z$ Complexes (%) as Obtained from the B3LYP DFT Calculations

complex	MO	(d_{yz})	(d_{xz})	(d_{xy})	S(p_z)	S($p_{x,y}$)	C(p_z)	C(p_s)
1	$2b_{3g}$	95						
	$2b_{2g}$		94					
3	$2b_{3g}$	82			7		10	
	$2b_{2g}$		71		22		7	
$[Co(bdt)_2]^{-}$ [a]	$2b_{3g}$	72			10		10	
	$2b_{2g}$		65		28		08	
$[\mathbf{3}^{Red}]^{2-}$	$2b_{3g}$	72			18		9	
	$2b_{2g}$		71		10		12	
	$3b_{2g}$		19		3		69	
$[Fe^{II}(bdt)_2]^{2-}$ [a]	$2b_{3g}$	90			3		2	
	$2b_{2g}$		82		8		6	
4	$1b_{2g}$		28		26		39	
	$1b_{1u}$				47		42	
	$2b_{2g}$		61		26		10	
$[\mathbf{4}^{Red}]^{3-}$	$2b_{3g}$	71			15		13	
	$2b_{2g}$		58		30		11	
	$2a_u$				9		87	
$[Ni^{II}(L)_2]^{2-}$ [b]	$2b_{3g}$	71			17			
	$2b_{2g}$		52		36			
	$1b_{1g}$			50		40		2

[a] Values taken from ref 20. [b] See also refs 28, 29.

Table 8. Experimental and Calculated Electronic Spectra of **4** and $[\mathbf{4}^{Red}]^{3-}$ and Assignments from TD-DFT (COSMO) Calculations at the ZORA-B3LYP Level (CH_2Cl_2 Solvent)

		transition energy, cm^{-1}		oscillator strength		
complex	band	exptl	calcd	exptl	calcd	assignment
4	I	13240	18710	0.10	0.16	$1b_{1u}(L) \rightarrow 2b_{2g}(d_{xz} + L)$
	II	14200	20960	0.03	0.08	$1a_u(L) \rightarrow 2b_{2g}(d_{xz} + L)$
	III	16300	20830	0.04	0.03	$2b_{2g}(d_{xz} + L) \rightarrow 2b_{1u}(L)$
$[\mathbf{4}^{Red}]^{3-}$	Ia	13300	12100	0.05	0.11	$2b_{2g}(d_{xz} + L) \rightarrow 2b_{1u}(L)$
	IIa	14420	17790	0.03	0.02	$2b_{2g}(d_{yz}) \rightarrow 2a_u(L)$
	IIIa	14970	14870	0.01	0.001	$1b_{3g}(d_{yz}) \rightarrow 2b_{1u}(L)$
	IVa	16560	14590	0.01	0.001	$2a_g(d_{z^2}) \rightarrow 2b_{1u}(L)$

When monoanionic **3** is reduced to $[\mathbf{3}^{Red}]^{2-}$, the extra electron populates the $1b_{3g}$ (d_{yz} + L) MO, which possesses 72% Co $3d_{yz}$ and 27% ligand character (Table 7). $[\mathbf{3}^{Red}]^{2-}$ possesses a $^2B_{2g}$ ground state. The $1b_{3g}$ orbital decreases considerably in energy as compared to that in **3**, and the $3b_{2g}$ orbital continues to be the SOMO (71% Co $3d_{xz}$; 22% ligand contribution). Thus, the reduction of **3** to $[\mathbf{3}^{Red}]^{2-}$ is a metal-centered process affording Co(II) (d^7 low-spin). The population of the $1b_{3g}$ orbital in **3** with an extra electron results in the destabilization of the $2a_g$ (d_{z^2}) orbital, which remains higher in energy than the $1a_g$ ($d_{x^2-y^2}$) orbital.

The electronic structure of the dianion in **4** shown in Figure 11 is found to be rather similar to that of $[\mathbf{3}^{Red}]^{2-}$ possessing the same $^2B_{2g}$ ground state electron configuration ($S = {}^1/_2$). The unpaired electron resides in a $2b_{2g}$ (d_{xz} + L) orbital in both compounds, showing only small differences in their metal and ligand orbital contributions (Table 7). The $2b_{2g}$ SOMO has 61% Rh $4d_{xz}$ and 36% ligand character; the spin density on the *n*d orbitals for $[\mathbf{3}^{Red}]^{2-}$ and **4** are 1.01 and 0.66, respectively.

A most notable change of the electronic structure is observed upon reduction of the paramagnetic dianion $[Rh^{II}(L)_2]^{2-}$ by one electron, yielding the square planar,

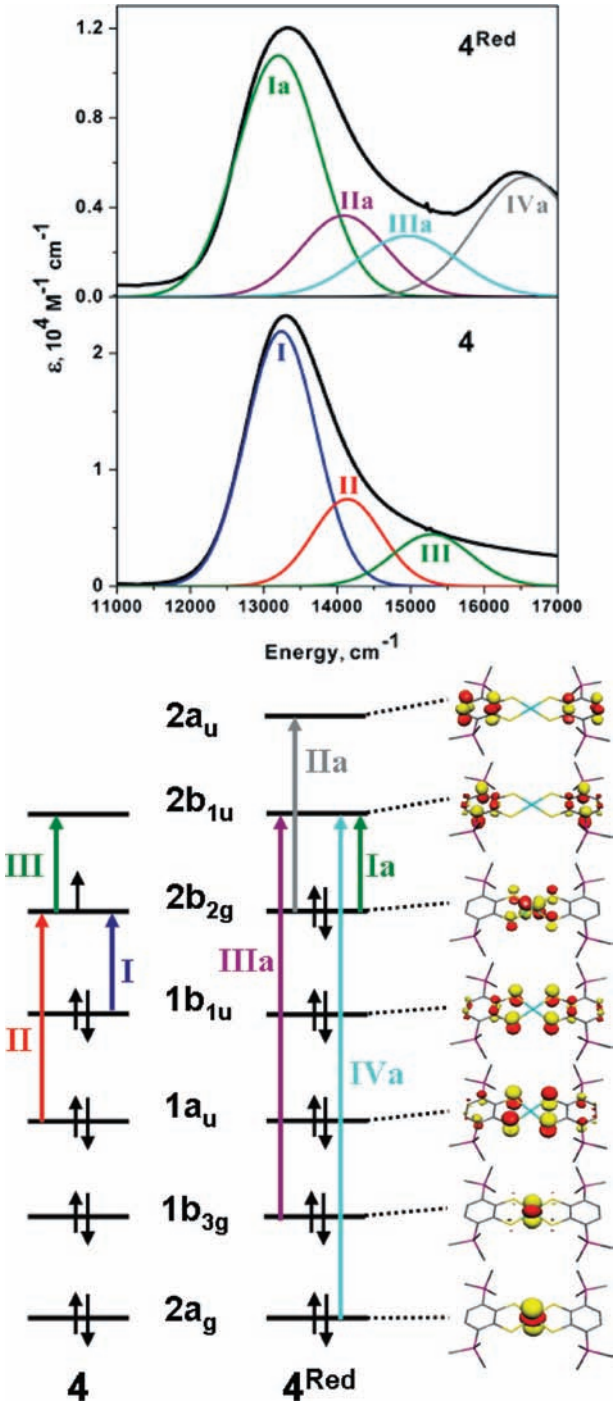

Figure 12. Experimental and deconvoluted electronic absorption spectra of $[Rh^{I}(L)_2]^{3-}$ ($\mathbf{4}^{Red}$) (top) and of $[Rh^{II}(L)_2]^{2-}$ (**4**) (bottom) and assignment of transitions as determined from TD-DFT calculations.

diamagnetic trianion $[Rh(L)_2]^{3-}$. Figure 11 exhibits a qualitative MO scheme from a ZORA-B3LYP DFT calculation for the trianion. Note that the metal 4d orbital energies are higher for the trianion than those for the dianion due to the lower effective nuclear charge of Rh(I). Upon reduction of the dianion, the additional electron populates the previously singly occupied $2b_{2g}$ orbital. In $[\mathbf{4}^{Red}]^{3-}$, this orbital is composed of equal contributions from the metal (58% Rh) and the ligands (41%). From the natural population analysis (Table 6), a total of 9.2 valence electrons have been calculated for the trianion

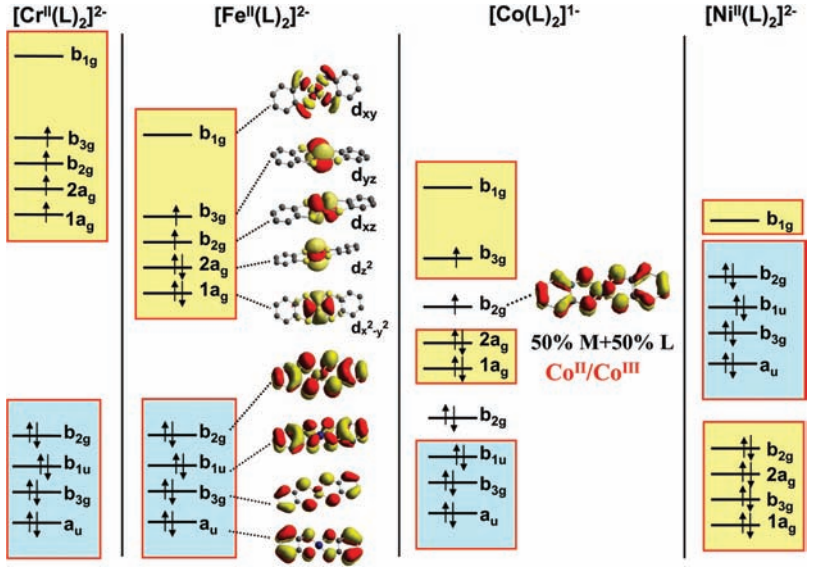

Figure 13. Comparison of qualitative MO schemes for $[Cr^{II}(L)_2]^{2-}$ (this work), $[Fe^{II}(L)_2]^{2-}$ (ref 20), $[Co(L)_2]^{-}$ (ref 28, 29), and $[Ni^{II}(L)_2]^{2-}$ (this work and ref 28), emphasizing the "normal" (Cr^{II}, Fe^{II}) and "inverted" (Ni^{II}),[30] and intermediate (Co^{III}) sequence of metal-based (yellow) and ligand-based (blue) orbitals as determined from DFT (B3LYP) calculations.

which—excluding the σ contributions to the unpopulated nd_{xy} orbital—results in 8.1 electrons, in agreement with a Rh(I) (d^8) ion.

9. Excited State Calculations and Assignments. Time-dependent DFT calculations of the electronic spectrum of $[Co(bdt)_2]^-$ in CH_2Cl_2 solution using the conductor-like screening model (COSMO)[27] have recently been reported in the 22 000−10 000 cm^{-1} range. As expected, the $1b_{1u}-2b_{2g}$ LMCT transition is the most intense band at 670 nm, which contributes to the observed blue color of the complex. Three other LMCT transitions have also been identified and assigned.[20]

Here, we used the same methodology to calculate the electronic spectra of **4** and $[\mathbf{4}^{Red}]^{3-}$. Table 8 summarizes the experimental and calculated spectra of **4** and $\mathbf{4}^{Red}$ in the range 11 000−17 000 cm^{-1}, and Figure 12 shows the deconvolution of the spectra of **4**. Three transitions, I, II, and III, are observed and assigned. The calculations have been performed using the COSMO model (CH_2Cl_2).

The most intense band I at 13 240 cm^{-1} (calcd at 18 710 cm^{-1}) is a LMCT band ($1b_{1u}\rightarrow 2b_{2g}$). Band II is a spin and electric dipole-allowed transition $1a_u\rightarrow 2b_{2g}$ at 14 200 cm^{-1} (calcd. 20 960 cm^{-1}), and band III at 16 300 cm^{-1} corresponds to a $2b_{2g}\rightarrow 2b_{1u}$ transition (calcd at 20 830 cm^{-1}). The calculated band energies are overestimated by ~4000 cm^{-1} compared with the experimental values. This is acceptable and has also been observed for the spectrum of $[Co(bdt)_2]^-$ in ref 20.

The deconvoluted spectrum of $[\mathbf{4}^{Red}]^{3-}$ in CH_2Cl_2 exhibits four bands in the visible region (Figure 12). The intense band Ia at 13 300 cm^{-1} (calcd at 12 100 cm^{-1}) is assigned as HOMO−LUMO transition $2b_{2g}\rightarrow 2b_{1u}$, which has metal-to-ligand charge transfer character (MLCT).

Conclusions

The most salient features of the present study may be summarized as follows:

(a) In square planar bis(dithiolato)metal complexes with a d^n electron configuration, where n is 4, 5, and 6, as in Cr^{II} ($S=2$), Mn^{III} ($S=2$),[31] Fe^{III} ($S={}^3/_2$),[32] Fe^{II} ($S=1$),[20] and Co(III) ($S=1$), the energies of the metal d orbitals are always higher than that of the ligand π orbitals. Therefore, the redox chemistry of these species is in general metal-centered, as is exemplified by the reduction of **3** and **4**, yielding $[\mathbf{3}^{Red}]^{2-}$, which encompasses a low-spin Co(II) ion (d^7, $S={}^1/_2$), and $[\mathbf{4}^{Red}]^{3-}$, which possesses a diamagnetic Rh(I) ion (d^8, $S=0$).

(b) This changes with decreasing effective nuclear charge of the central transition metal ion. Thus, some $[CoL_2]^-$ complexes possess a electronic structure where the ligand π and metal d orbitals are similar in energy, and consequently, an unambiguous assignment of the metal (or ligand) oxidation level is not meaningful.[20] We note that the SOMOs in **3** ($S=1$) possess predominantly metal d character, and therefore, an assignment as intermediate spin Co(III) is appropriate.

(c) As has been noted previously[29,30] in $[Ni^{II}L_2]^{2-}$ (Ni(II), d^8, $S=0$) species, the HOMO is predominantly a ligand-centered π orbital. This is schematically summarized in Figure 13. For these "inverted" species,[30] the redox chemistry is therefore ligand-centered.

Acknowledgment. We thank the Fonds der Chemischen Industrie for financial support. F.L.B. gratefully

(27) Klamt, A.; Schüürmann, G. *J. Chem. Soc., Perkin Trans.* **1993**, *2*, 799.
(28) Ray, K.; DeBeer George, S.; Solomon, E. I.; Wieghardt, K.; Neese, F. *Chem.—Eur. J.* **2007**, *13*, 2783.
(29) Ray, K.; Petrenko, T.; Wieghardt, K.; Neese, F. *Dalton Trans.* **2007**, 1552.
(30) Szilagyi, R. K.; Lim, B. S.; Glaser, T.; Holm, R. H.; Hedman, B.; Hodgson, K. O.; Solomon, E. I. *J. Am. Chem. Soc.* **2003**, *125*, 9158.
(31) (a) Greiwe, K.; Krebs, B.; Henkel, G. *Inorg. Chem.* **1989**, *28*, 3713. (b) Henkel, G.; Greiwe, K.; Krebs, B. *Angew. Chem., Int. Ed. Engl.* **1985**, *24*, 117.
(32) Roy, N.; Sproules, S.; Bill, E.; Weyhermüller, T.; Wieghardt, K. *Inorg. Chem.* **2008**, *47*, 10911.

acknowledges the Max Planck Society for a stipend. The authors thank Dr. Carsten Milsmann for valuable discussions.

Note Added after ASAP Publication. Due to a production error, this paper was released ASAP on October 15, 2009, before the author corrections were implemented. The corrected version was posted on November 6, 2009.

Supporting Information Available: X-ray crystallographic files in CIF format; crystallographic results for $[L'L''Rh(I)_2]_{0\cdot7}/[L'L''Rh(I)(CH_3)]_{0\cdot3}$ (atom coordinates, bond lengths and angles, thermal parameters; and calculated hydrogen atom coordinates. Table S6 of calculated and experimental bond lengths in **1**, **2**, **3**, $[\mathbf{3}^{Red}]^{2-}$, **4** $[\mathbf{4}^{Red}]^{3-}$, and $[NiL_2]^{2-}$. This material is available free of charge via the Internet at http://pubs.acs.org.